Supplementary Materials

Reconstruction-mediated interfacial water engineering in Cu-Mo electrocatalyst for highly efficient and durable water splitting

Jianfang Zhang[1,2,#], Jiapei Li[2,#], Yan Wang[1,*], Miao Han[1], Chuhao Luan[2], Shuai Xia[1], Cuiping Yu[1], Yucheng Wu[1,3,*], Wenjun Zhang[2,*]

[1]School of Materials Science and Engineering, Hefei University of Technology, Hefei 230009, Anhui, China.

[2]Department of Materials Science and Engineering & Center of Super-Diamond and Advanced Films (COSDAF), City University of Hong Kong, Kowloon, Hong Kong 99907, China.

[3]China International S&T Cooperation Base for Advanced Energy and Environmental Materials & Anhui Provincial International S&T Cooperation Base for Advanced Energy Materials, Key Laboratory of Advanced Functional Materials and Devices of Anhui Province, Hefei University of Technology, Hefei 230009, Anhui, China.

[#]Authors contributed equally.

Correspondence to: Dr. Yan Wang, School of Materials Science and Engineering, Hefei University of Technology, Hefei 230009, Anhui, China. E-mail: stone@hfut.edu.cn; Dr. Yucheng Wu, School of Materials Science and Engineering, Hefei University of Technology, Hefei 230009, Anhui, China; China International S&T Cooperation Base for Advanced Energy and Environmental Materials & Anhui Provincial International S&T Cooperation Base for Advanced Energy Materials, Key Laboratory of Advanced Functional Materials and Devices of Anhui Province, Hefei University of Technology, Hefei 230009, Anhui, China. E-mail: ycwu@hfut.edu.cn; Dr. Wenjun Zhang, Department of Materials Science and Engineering & Center of Super-Diamond and Advanced Films (COSDAF), City University of Hong Kong, Kowloon, Hong Kong 99907, China. E-mail: apwjzh@cityu.edu.hk

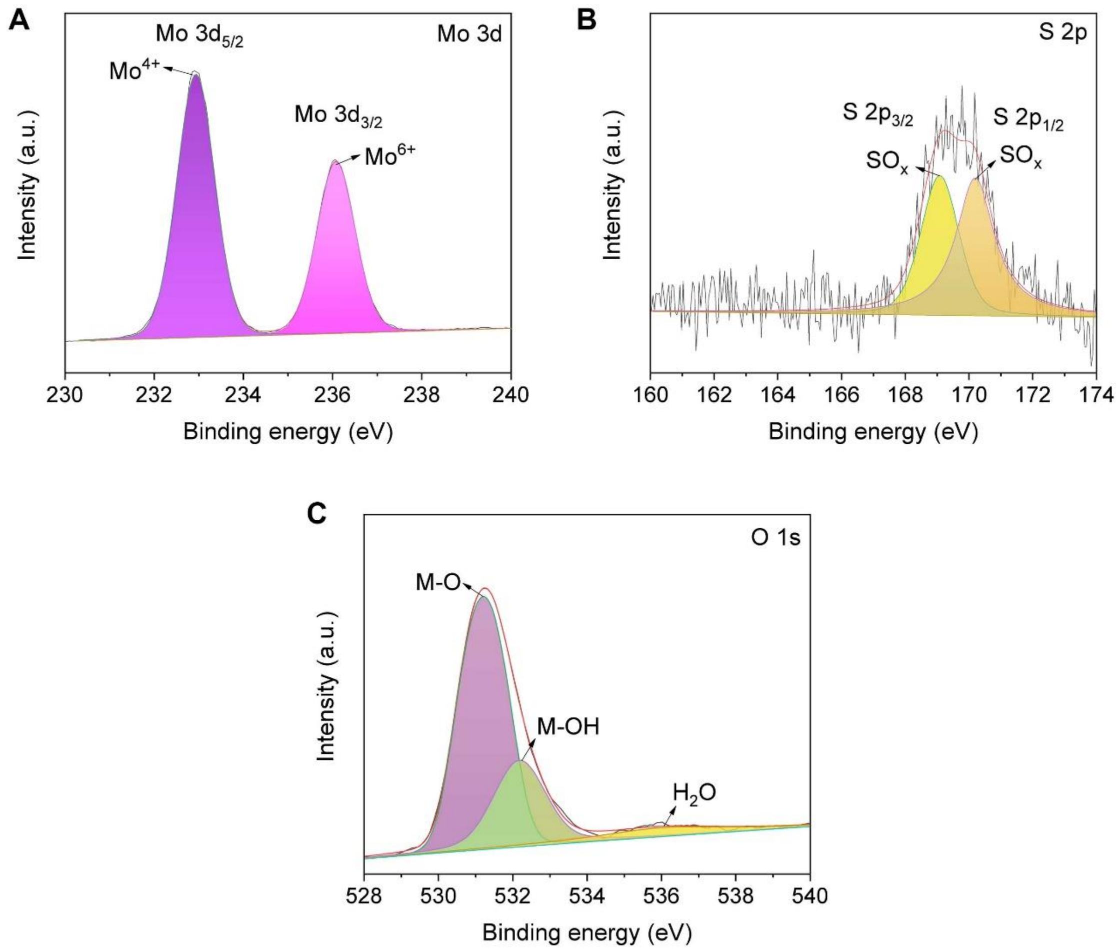

Supplementary Figure 1. XPS spectra of (A) Mo 3d, (B) S 2p, and (C) O 1s for MoS_2/MoO_3 nanosheets.

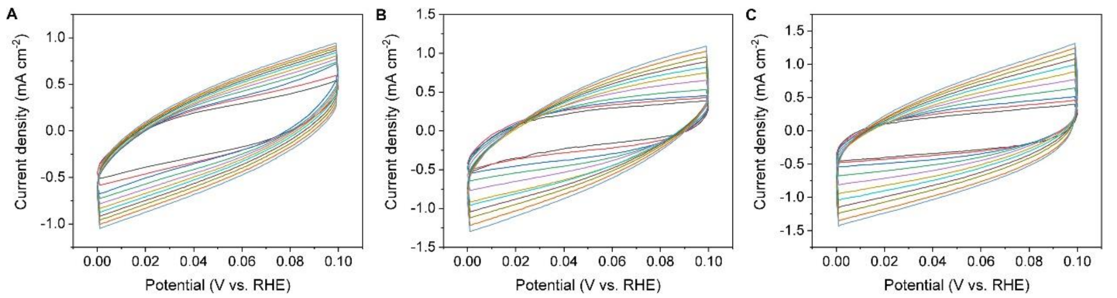

Supplementary Figure 2. CV curves of (A) Cu, (B) MoS_2, and (C) Cu-MoS_2 for HER under different scan rates from 10 to 200 mV s^{-1}.

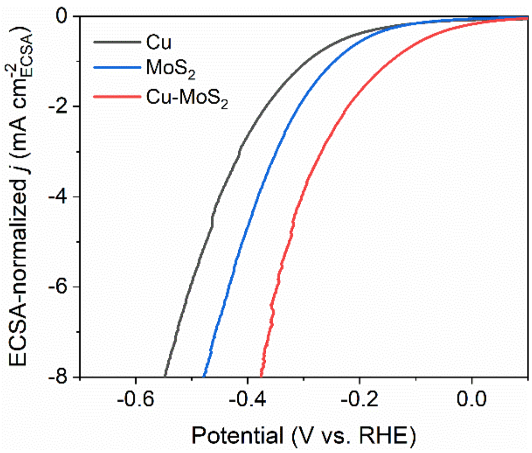

Supplementary Figure 3. ECSA-normalized current density of Cu-MoS_2 and control catalysts for HER.

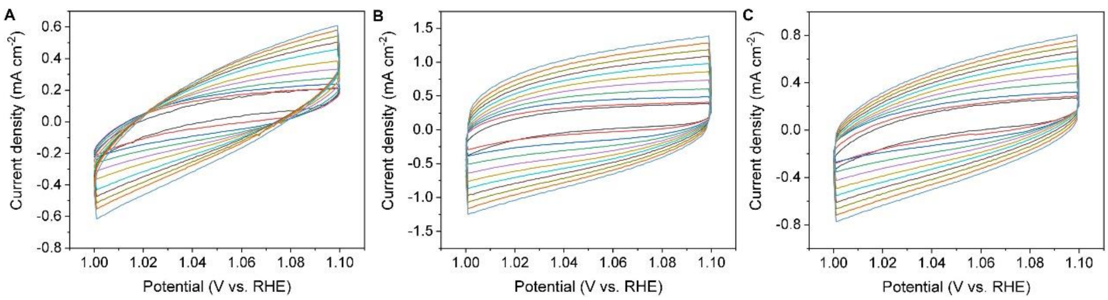

Supplementary Figure 4. CV curves of (A) CuO, (B) MoS_2/MoO_3, and (C) CuO-MoS_2/MoO_3 for OER under different scan rates from 10 to 200 mV s^{-1}.

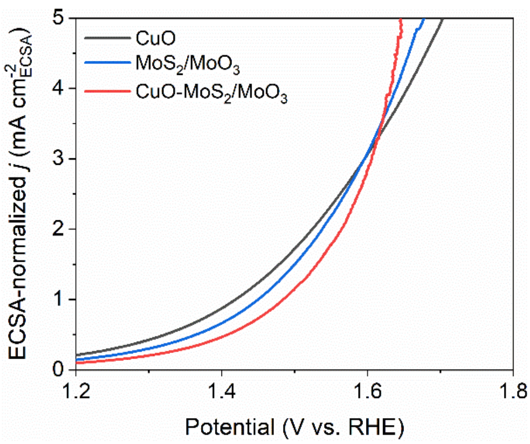

Supplementary Figure 5. ECSA-normalized current density of CuO-MoS_2/MoO_3 and control catalysts for OER.

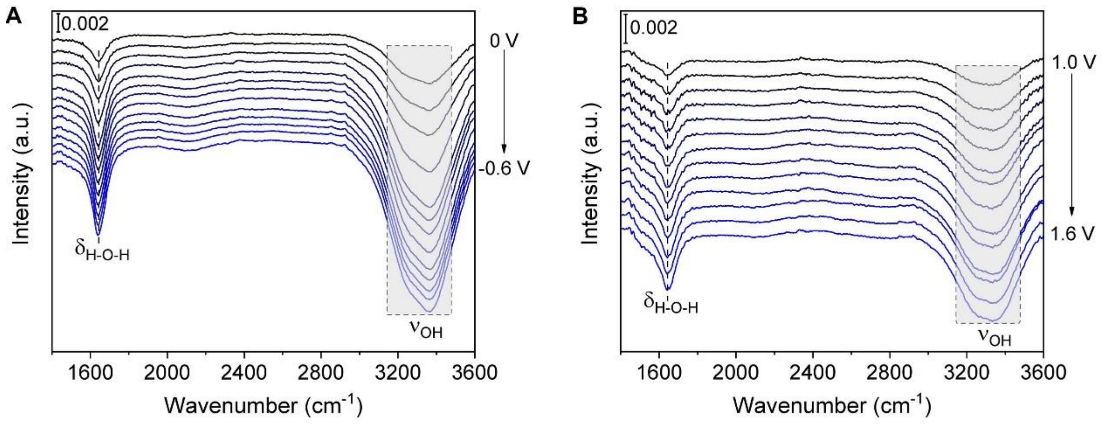

Supplementary Figure 6. In situ FTIR spectra of (A) Cu-MoS_2 for HER under the potential from 0 to -0.6 V and (B) CuO-MoS_2/MoO_3 for OER under the potential from 1.0 to 1.6 V.

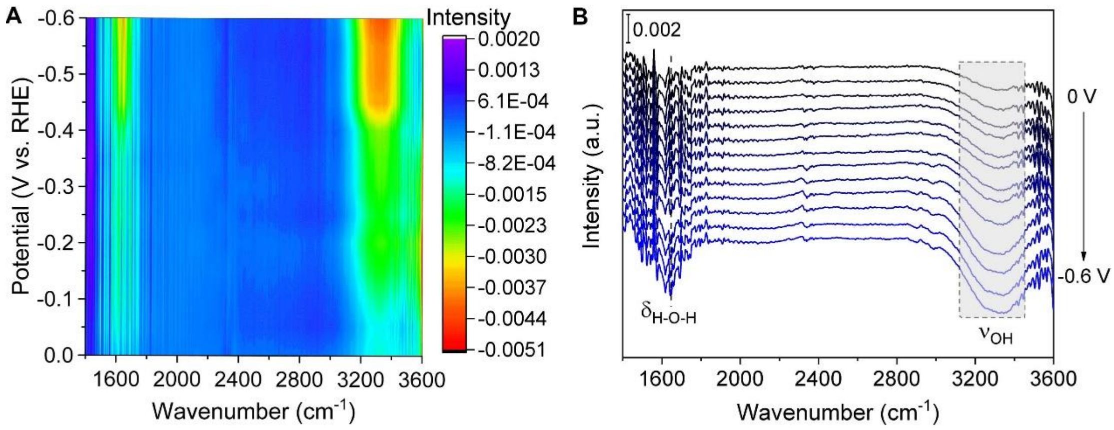

Supplementary Figure 7. In situ FTIR spectra of MoS_2 for HER under the potential from 0 to -0.6 V.

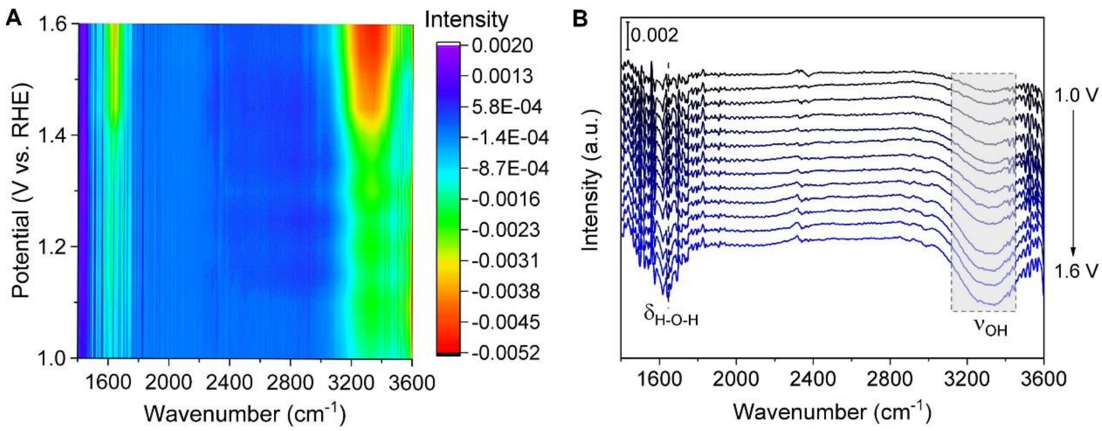

Supplementary Figure 8. In situ FTIR spectra of MoS_2/MoO_3 for OER under the potential from 1.0 to 1.6 V.

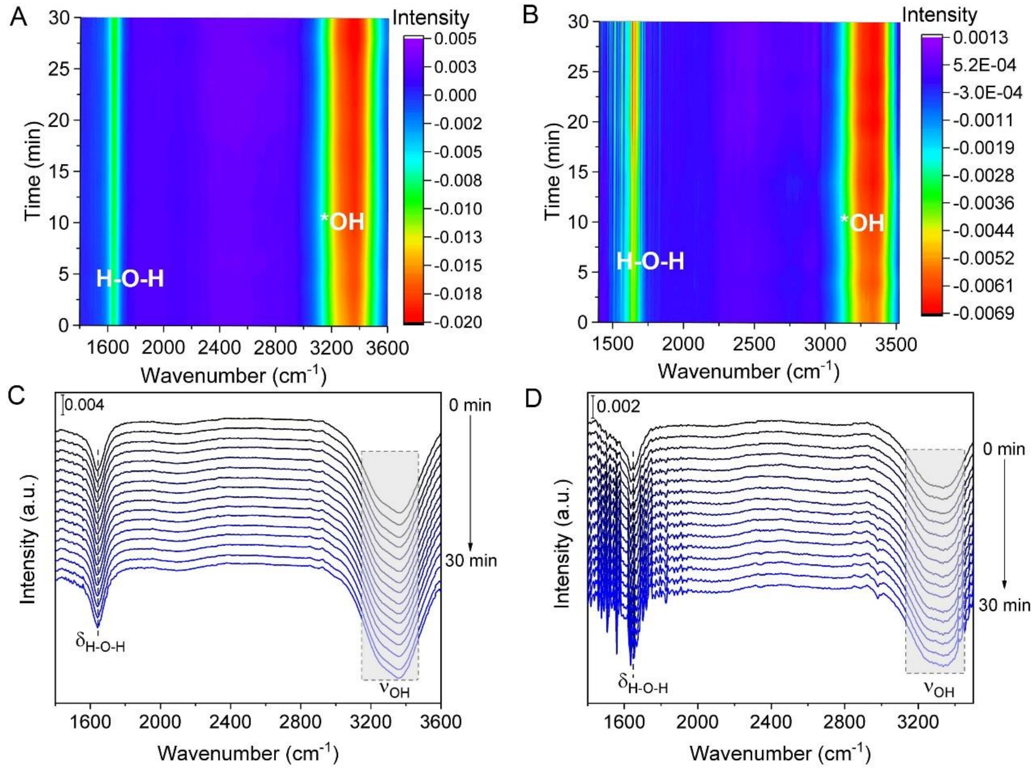

Supplementary Figure 9. Time-dependent in situ FTIR spectra of (A, C) Cu-MoS_2 for HER under a potential of -0.5 V for 30 min, and (B, D) CuO-MoS_2/MoO_3 for OER under a potential of 1.5 V for 30 min.

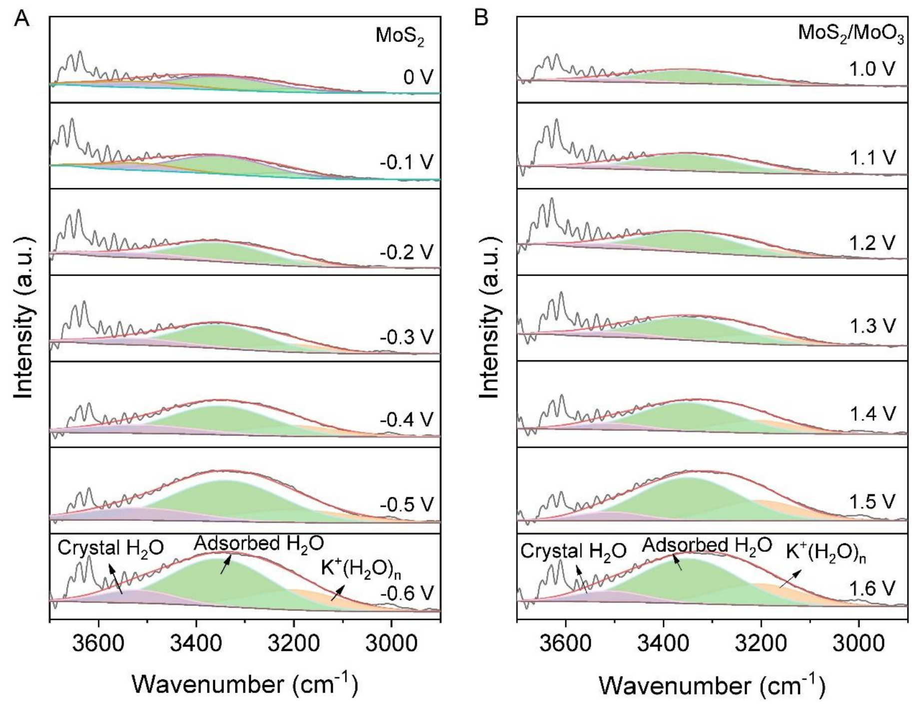

Supplementary Figure 10. The Gaussian fits of three O-H stretching modes on (A) MoS_2 and (B) MoS_2/MoO_3.

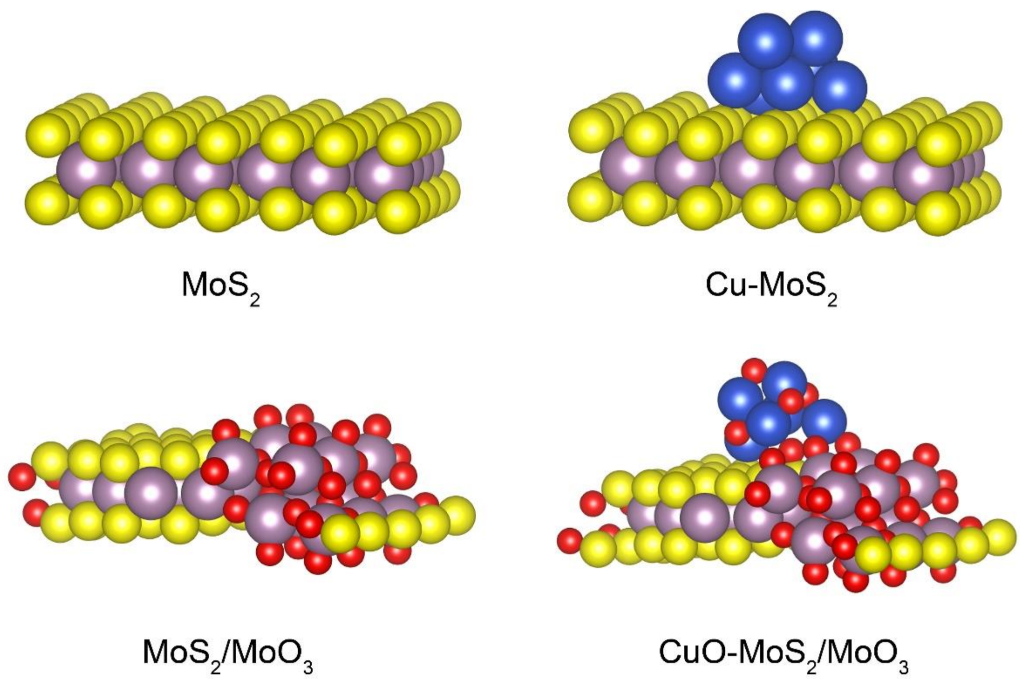

Supplementary Figure 11. Structural models of MoS_2, Cu-MoS_2, MoS_2/MoO_3, and CuO-MoS_2/MoO_3.

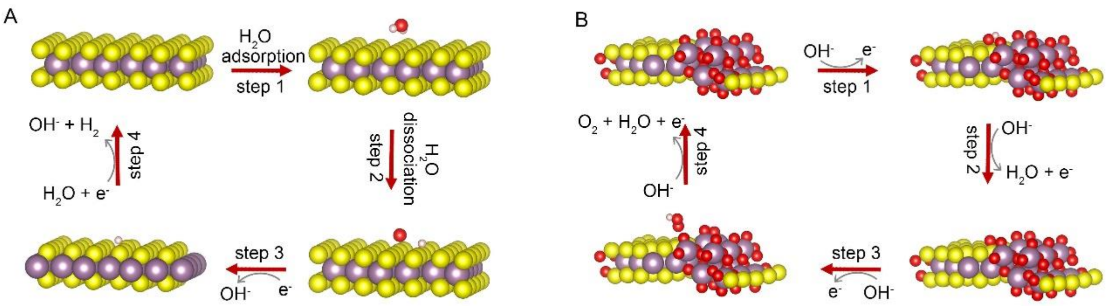

Supplementary Figure 12. Reaction pathways of (A) HER process on MoS_2 and (B) OER process on MoS_2/MoO_3.

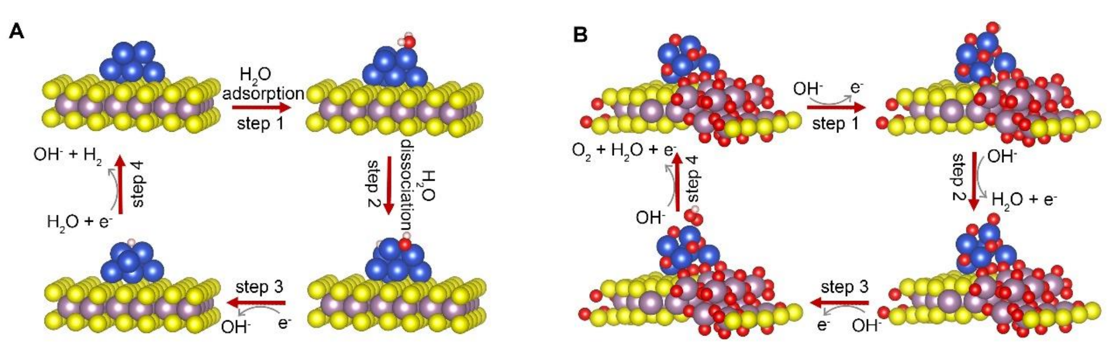

Supplementary Figure 13. Reaction pathways of (A) HER process on Cu-MoS_2 at Cu site and (B) OER process on CuO-MoS_2/MoO_3 at CuO site.

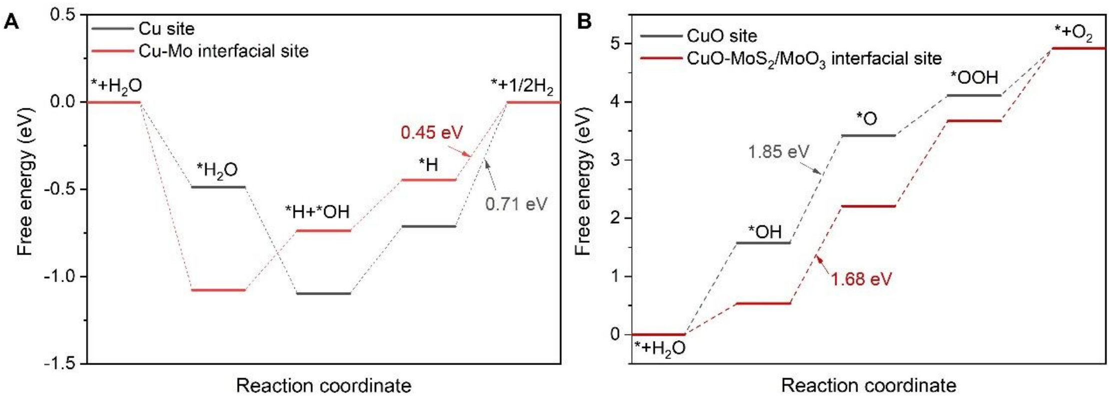

Supplementary Figure 14. Gibbs free energy diagram for (A) HER process on Cu-MoS_2 at Cu site and Cu-Mo interfacial site, and (B) OER process on CuO-MoS_2/MoO_3 at CuO site and CuO-MoS_2/MoO_3 interfacial site.

Supplementary Table 1. ECSA-normalized activity, turnover frequency (TOF), and mass activity for HER.

Catalysts	ECSA	j_{ECSA} (mA cm^{-2}_{ECSA})		TOF (s^{-1})		Mass activity (A g^{-1})	
		η=100 mV	η=500 mV	η=100 mV	η=500 mV	η=100 mV	η=500 mV
Cu	77.75	0.153	5.92	0.48	18.5	23.8	920.6
MoS_2	109.25	0.155	8.97	0.48	28.0	34.0	1969.8
Cu-MoS_2	143.25	0.611	8.94	1.91	27.9	175.2	2562.3

Supplementary Table 2. ECSA-normalized activity, turnover frequency (TOF), and mass activity for OER.

Catalysts	ECSA	j_{ECSA} (mA cm^{-2}_{ECSA})		TOF (s^{-1})		Mass activity (A g^{-1})	
		η=200 mV	η=500 mV	η=200 mV	η=500 mV	η=200 mV	η=500 mV
CuO	55.75	1.078	5.594	0.168	0.870	120.2	623.7
MoS_2/MoO_3	104.50	0.847	6.731	0.132	1.052	176.9	1406.8
CuO-MoS_2/MoO_3	204.25	0.612	5.981	0.095	0.932	250.0	2442.8

Supplementary Table 3. Comparison of the performance of the Cu-MoS_2||CuO-MoS_2/MoO_3 electrolyzer with reported electrolyzers.

Electrolyzer		Temperature (°C)	Cell voltage (V) @ 1.0 A cm^{-2}	Stability (h)	Ref.
Cathode	Anode				
Cu-MoS_2	CuO-MoS_2/MoO_3	80	1.77	500	This work
$Ru_{8\%}$-Co_3O_4	$Ru_{8\%}$-Co_3O_4	85	2.06	120	[1]
MCHEP	MCHEP	80	1.83	400	[2]
Ru,Mn-NiCoP	Ru,Mn-NiCo LDH	85	2.0	80	[3]
Ir_{SA}-NiFe LDH/NiMo	Ir_{SA}-NiFe LDH/NiMo	60	1.72	120	[4]
FeO_x@$Co_{0.75}Fe_{0.25}P$	FeO_x@$Co_{0.75}Fe_{0.25}P$	60	1.73	120	[5]
NiMn-OPSe	NiMn-OPSe	70	2.07	500	[6]
NiFe@Ni/Fe-MnOOH	NiFe@Ni/Fe-MnOOH	25	1.953	200	[7]
$Ni(OH)_2$@$Pt^{\delta-}$-NC	NiFe-LDH	25	1.78	200	[8]
Pt-C core-shell @*h*-MoS_2/GNF	$NiCo_2O_4$	60	2.18	15	[9]
Y-NiMo/MoO_{2-x}	NiFe-LDHs	80	1.78	24	[10]
NiFeCu	NiFeCu	25	2.13	12	[11]
Ir-$Ni(OH)_2$/NF	Ir-$Ni(OH)_2$/NF	60	1.64	225	[12]
HS Co_3S_4	Mo-CoOOH	60	1.78	1000	[13]
Ni_2P@FeP@Co_2P	Ni_2P@FeP@Co_2P	85	1.95	500	[14]
Pt/C	NiFe-LDH-PTA	60	1.93	170	[15]
$Co_2Mo_3O_8$/MoO_2/NF	FeMoOOH/NF	65	1.76	75	[16]
P-Os/NiFe	RuO_2/NiFe	60	2.02	100	[17]
$Er_{0.1}$-CoP/NiCoP@NF	Ce-Fe_xP/Ni_3P@NF	50	1.783	1000	[18]
Ru-Ru_2P/V_2CT_x	RuO_2	75	1.80	550	[19]

Cu-$MoNi_4$@NF	NiFeOOH	60	1.74	1000	[20]
N-NiMo/MoO_2	NiFe	80	1.87	120	[21]
Cu/Ni@MoO_2	NiFeOOH	60	1.69	1000	[22]
Pt/C	Mo-doped Ni_3S_2/$FeNi_2S_4$	60	1.66	200	[23]
NiSe	r-$NiMoSe_x$	80	1.70	190	[24]
Ni@Ti-MoO_x	NiFe LDH	60	1.72	100	[25]
Cr-NiMo/MoO_2	Ni_3S_2–NiFe LDH	80	1.74	30	[26]
Mo_2C/NiMo	Mo_2C/FeNiMo	60	~1.78	100	[27]
Ru-MoN_4-NC	NiFe LDH	60	1.72	1200	[28]
NiRu-MOF	FeNi-MOF	25	2.00	350	[29]
Os SA/NiCu	NiFe LDH	80	1.76	500	[30]

References

1. Zhou, Y.; Mao, Y.; Ye, C., et al., Ru single atoms anchored on Co_3O_4 nanorods for efficient overall water splitting under pH-universal conditions. *Adv. Energy Mater.* **2025,** *15*, 2500700. DOI: 10.1002/aenm.202500700.
2. Li, J.; Hu, J.; Chen, C., et al., Nitrogen-doped carbon shells and MXene double-confined high-entropy phosphates for robust anion exchange membrane water electrocatalysis. *Chem. Eng. J.* **2025,** *522*, 167854. DOI: 10.1016/j.cej.2025.167854.
3. Ma, W.; Zhang, Y.; Wang, B., et al., Significantly enhanced OER and HER performance of NiCo-LDH and NiCoP under industrial water splitting conditions through Ru and Mn bimetallic co-doping strategy. *Chem. Eng. J.* **2024,** *494*, 153212. DOI: 10.1016/j.cej.2024.153212.
4. Wu, Y.; Chen, M.; Sun, H., et al., Coupling Ir single atom with NiFe LDH/NiMo heterointerface toward efficient and durable water splitting at large current density. *Appl. Catal. B: Environ.* **2025,** *360*, 124548. DOI: 10.1016/j.apcatb.2024.124548
5. Wen, N.; Wang, H.; Liu, Q., et al., Field-effect eenhancement of non-Faradaic processes at interfaces governs electrocatalytic water splitting activity. *Adv. Sci.* **2024,** *11*, e2403206. DOI: 10.1002/advs.202403206.
6. Nguyen, H. T.; Majumdar, A.; Nguyen, T. T. A., et al., Interface engineering of defected earth-abundant transition metal oxo-phospho-selenide-derived electrocatalyst for high-performance AEM water electrolysis. *J. Colloid. Interface Sci.* **2026,** *701*, 138703. DOI: 10.1016/j.jcis.2025.138703.
7. Feng, M.; Tang, Y.; Li, Z., et al., Differentiated modulating the electronic structure of NiFe@Ni/Fe-MnO_x via phase transformation engineering to synergy promote bifunctional water splitting reactions. *Small* **2025,** *21*, e2410752. DOI: 10.1002/smll.202410752.

8. Li, J.; Li, H.; Xie, W., et al., Scalable and facile flame-assisted synthesis of electron-rich Pt clusters/$Ni(OH)_2$ electrocatalyst for robust AEM water electrolysis. *Matter* **2025**, 102414. DOI: 10.1016/j.matt.2025.102414.
9. Ramakrishnan, S.; Vijayapradeep, S.; Selvaraj, S. C., et al., An efficient cathode electrocatalyst for anion exchange membrane water electrolyzer. *Carbon* **2024,** *220*, 118816. DOI: 10.1016/j.carbon.2024.118816.
10. Liu, S.; Zhang, Z.; Dastafkan, K., et al., Yttrium-doped NiMo-MoO_2 heterostructure electrocatalysts for hydrogen production from alkaline seawater. *Nat. Commun.* **2025,** *16*, 773. DOI: 10.1038/s41467-025-55856-4.
11. Zhang, Z.; Wan, S.; Wang, H., et al., Electrochemical synthesis of trimetallic nickel-iron-copper nanoparticles via potential-cycling for high current density anion exchange membrane water-splitting applications. *J. Energy Chem.* **2024,** *89*, 535-542. DOI: 10.1016/j.jechem.2023.10.033.
12. Wan, R.; Wang, Y.; Wu, X., et al., Iridium single-atom-modulated nickel hydroxide for boosting overall water splitting. *ACS Nano* **2025,** *19*, 38849-38860. DOI: 10.1021/acsnano.5c15995.
13. Long, Y.; Zhao, S.; Wang, L., et al., Regulating high electron spin state in Co_3S_4 for enhanced water splitting. *ACS Catal.* **2025,** *15*, 9845-9855. DOI: 10.1021/acscatal.4c07849.
14. Ma, W.; Zhang, Y.; Hu, L., et al., Dynamic restructuring of asymmetric built-in electric field catalysts facilitates the efficient water splitting. *Adv. Funct. Mater.* **2025,** *35*, 2422734. DOI: 10.1002/adfm.202422734.
15. Zhang, J.; Zhang, X.; Ma, Z., et al., POM-intercalated NiFe-LDH as enhanced OER catalyst for highly efficient and durable water electrolysis at ampere-scale current densities. *ACS Catal.* **2025,** *15*, 6486-6496. DOI: 10.1021/acscatal.5c00448.
16. Sun, J.; Zhou, S.; Zhao, Z., et al., Deep reconstruction of a Mo-based electrocatalyst for high-performance water/seawater oxidation at ampere-level current density. *Energy Environ. Sci.* **2025,** *18*, 1952-1962. DOI: 10.1039/d4ee04941a.
17. Li, Q.; Fu, X.; Li, H., et al., Strong d-p orbital hybridization of Os-P via ultrafast microwave plasma assistance for anion exchange membrane electrolysis. *Adv. Funct. Mater.* **2024,** *34*, 2408517. DOI: 10.1002/adfm.202408517.
18. Zhang, F.; Zhang, H.; Han, W., et al., Synergistic modulation of multisite electronic states via erbium doping and NiCoP hybridization for enhanced anion exchange membrane water splitting. *Nano Lett.* **2025,** *25*, 4441-4449. DOI: 10.1021/acs.nanolett.5c00001.
19. Nguyen, T. H.; Tran, P. K. L.; Tran, D. T., et al., Ru-Ru_2P hetero-cluster promoted V_2CTx sheets-based electrocatalyst enables industrial-level AEM water electrolysis. *Appl. Catal. B: Environ.* **2024,** *343*, 123517. DOI: 10.1016/j.apcatb.2023.123517.
20. Sun, J.; Zhong, L.; Chen, S.; et al. Micro-galvanic-driven scalable synthesis of heterostructured nanoarrays for durable anion exchange membrane water electrolysis. *Small* **2025**, *21*, 2503794. DOI: 10.1002/smll.202503794.
21. Sun, Y.; Qi, M.; Tan, X.; et al. Gram-scale synthesis of N-NiMo/MoO_2 heterostructures to boost hydrogen evolution in low-alkalinity anion exchange membrane water electrolysis. *Nano Energy* **2025**, *146*, 111489. DOI: 10.1016/j.nanoen.2025.111489.
22. Zhong, L.; Li, Y.; Zheng, L.; et al. Cu-mediated proximal electronic engineering in Ni/MoO_2 heterostructures for industrial alkaline hydrogen evolution. *Chem. Eng.*

J. **2025**, *526*, 170806. DOI: 10.1016/j.cej.2025.170806.

23. Patil, K.; Lee, J.; Choi, D.; et al. Interfacial engineering of Mo-doped $Ni_3S_2/FeNi_2S_4$ heterostructures for durable industrial-level current-density AEM water electrolysis. *J. Mater. Chem. A* **2026**, *14*, 506–520. DOI: 10.1039/d5ta08510a.
24. Qin, R.; Yao, Q.; Zeng, W.; et al. Facile reconstruction of Se-regulated NiMo nanorods for efficient anion exchange membrane water electrolysis. *Nano Lett.* **2025**, *25*, 4979–4986. DOI: 10.1021/acs.nanolett.5c00347.
25. Wang, R.; Yin, X.; Xiao, J.; et al. Topological engineering of NiMo cathode catalyst for efficient anion exchange membrane water electrolysis. *J. Alloys Comp.* **2026**, *1067*, 188402. DOI: 10.1016/j.jallcom.2026.188402.
26. Li, C.; Zhang, K.; Zhao, R.; et al. Rational manipulation of built-in electric field strength and interfacial water structure in Cr-doped $NiMo/MoO_2$ nanotube arrays for superior aemwe hydrogen evolution at ampere-level current densities. *Appl. Catal. B: Environ.* **2026**, 127242. DOI: 10.1016/j.apcatb.2026.127242.
27. Lee, K.-A.; Ting, Y.-C.; Chang, C.-W.; et al. Interfacial electron transfer-driven activity enhancements of carbide/alloy heterostructured catalysts toward water electrolysis for high-performance anion exchange membrane water electrolysis. *J. Mater. Chem. A* **2026**, *14*, 25755–25770. DOI: 10.1039/d6ta02888h.
28. Han, S.; Wang, X.; Bao, J.; et al. Single-atom Mo with high oxophilicity anchored Ru clusters for practical anion-exchange-membrane water electrolyzer. *Adv. Funct. Mater.* **2025**, *36*, e22524. DOI: 10.1002/adfm.202522524.
29. Wei, S.; Wang, Y.; Zhou, J.; et al. Triangular motif engineering in metal-organic frameworks enables ampere-level anion exchange membrane water electrolysis. *Mater. Today Energy* **2026**, *59*, 102306. DOI: 10.1016/j.mtener.2026.102306.
30. Li, Y.; Zhao, P.; Huang, J.; et al. Tailored design of engineered Os-SA/NiCu single-atom alloys for sustainable anion exchange membrane water electrolysis. *Chem. Eng. J.* **2026**, *543*, 178241. DOI: 10.1016/j.cej.2026.178241.